Rock Mechanics and Rock Engineering
https://doi.org/10.1007/s00603-023-03350-y

ORIGINAL PAPER

Study Under X-Ray Tomography of the Impact of Self-Sealing Process on the Permeability of the Callovo-Oxfordian Claystone

M. Agboli[1] · D. Grgic[1] · M. Moumni[1] · A. Giraud[1]

Received: 28 November 2022 / Accepted: 19 April 2023

Abstract
To analyze the self-sealing process in the Callovo-Oxfordian claystone, self-sealing tests were performed on initially fractured samples under different temperatures with water and gas injection. Cylindrical samples oriented in parallel and perpendicularly to the bedding plane with an artificial initial fracture were used in a triaxial compression cell transparent to X-rays. Water and gas permeability were measured and the evolution of cracks volume was analyzed from X-ray tomography 3D images to characterize the self-sealing process. All tests performed at 20 °C with water injection showed a rapid drop in permeability at the beginning followed by a progressive decrease and a stabilization after one month. The permeability of fractured samples decreases significantly after self-sealing but is still higher (by 2 orders of magnitude) than the permeability of healthy claystone. Otherwise, the less calcite the sample contains (i.e., the more clayey it is), the faster the crack self-seals. The smaller the opening of the initial crack is, the faster the water permeability decreases and the crack closes. No significant influence of the sample orientation on the self-sealing kinetic was identified at this stage. It seems that high temperature has a slight retarding effect on the self-sealing process. For the test with water and gas injection, the injection of gas delays the decrease of water permeability and the self-sealing process, which is probably due to the crack desaturation induced by gas injection.

Highlights

- Self-sealing tests were performed on initially fractured samples of Callovo-Oxfordian claystone with different temperatures, orientations and fluids (water, gas).
- Self-sealing process was analyzed thanks to permeability measurements and crack volume estimation from X-ray tomography 3D images.
- The self-sealing process is fast at the beginning of the test and stabilizes after about one month and the initial permeability of the healthy rock is partially restored.
- The less calcite the sample contains (the more clayey it is) and the smaller the opening of the initial crack is, the faster the crack self-seals.
- Temperature and gas seem to have a delay effect on the self-sealing process. There is no significant influence of the sample orientation.

Keywords Self-sealing · X-ray tomography · Claystone · Gas and water permeability · Temperature

D. Grgic
dragan.grgic@univ-lorraine.fr

1 Laboratoire GeoRessources, Université de Lorraine, CNRS, 54000 Nancy, France

Published online: 03 May 2023

1 Introduction

Excavation of underground galleries in rocks creates a network of cracks near the excavation zone called an Excavation Damaged Zone (EDZ). In the Underground Research Laboratory (URL) of the National Agency of Radioactive waste Management (ANDRA) located in Meuse/Haute-Marne (Bure, France) and excavated in the Callovo-Oxfordian (COx) claystone, EDZs have been observed. This network of cracks desaturates the claystone and causes it to lose its mechanical and hydraulic (i.e., sealing) properties. But it was noted that during the resaturation of structures, the fractures generated during the excavation can self-seal and cause both a significant decrease in water permeability in the EDZ and a partial restoration of the mechanical properties of the rock (Bock et al. 2010). That phenomenon was called self-sealing. In the context of radioactive waste disposal, knowing the long-term behavior of the damaged area over time is of great importance.

Sealing is the reduction of fracture permeability by any hydromechanical, hydrochemical or hydrobiochemical processes in the EDZ (Bastiaens et al. 2007). In contrast to healing, sealing is characterized by only part of the restoration of the initial rock properties. Healing corresponds to sealing with loss of memory of the pre-healing state; thus the healed fracture will not be a preferred site for new fracturing just because of its history (Bastiaens et al. 2007). Several authors have studied the phenomenon of cracks self-sealing in claystones induced by the percolation of water. For Auvray et al. (2015), self-sealing is a result of a rearrangement of minerals and porosity in the fracture region. For these authors, there are three main processes involved. The first is swelling between sheets of smectite phases (intra-particle swelling), the second is inter-particle swelling due to osmotic effects, and the last is plugging or blockage of the fractures by particle aggregation. These processes lead to structural rearrangement within the self-sealed zone, which in turn determines the hydromechanical and transfer properties of the sealed fracture zone. Furthermore, Bastiaens et al. (2007) and Van Geet et al. (2008) proposed a synthesis of several in situ experiments on Opalinus clay (indurated claystone) and Boom clay (plastic claystone) presenting the capabilities of these clays to self-seal rather than self-restore. Concerning the Callovo-Oxfordian claystone, De La Vaissière et al. (2015) have shown the partial restoration of its permeability during in situ resaturation experiments. Over a one-year resaturation period, the hydraulic conductivity measured in the boreholes decreased by up to four orders of magnitude, approaching, but not reaching, the value of the healthy claystone. This result illustrated the ability of the COx claystone to self-seal.

The ability of claystone to self-seal has then been proven by several authors, but there are very little information on the self-sealing process when the crack is subjected to different temperatures and fluids. Auvray et al. (2015) performed self-sealing tests on the COx argillite in a PEEK triaxial cell under room temperature but with only 2D X-ray scans. Giot et al. (2019) performed the same kind of tests with 3D X-ray scans but with a limited amount of data and basic voxel data analysis. The objective of our study is to analyze the impact of temperature, calcite content, sample orientation, initial crack width and gas injection on the self-sealing process of artificial cracks in core samples of the COx claystone. To achieve these objectives, 2 kinds of self-sealing tests on the COx claystone will be performed. First, self-sealing tests with water injection under different temperatures, calcite contents, sample orientations and initial crack openings. Second, a mixed self-sealing test with injection of both water and gas. 3D X-ray scans will be performed on all tested samples before, during and after the experiment and the voxel data will be analyzed with a high-end software for the visualization and analysis of computed tomography (CT) data to estimate the evolution of the crack volume. In addition, water and gas permeability will be measured continuously during all tests. To our knowledge, there are no similar studies in the literature that characterize the self-sealing process in clay host rocks under such different and complex conditions.

2 Material and Methods

2.1 Description of the Studied Claystone

Claystone is a clayey rock that has suitable properties for radioactive waste storage. We focus on the Callovo-Oxfordian (COx) claystone, which is the host rock chosen in France for the storage of radioactive waste more precisely in Meuse/Haute-Marne (Bure, France). It is 160 million years old and, with a thickness of about 130 m, and located under Bure at a depth of 400 to 600 m. The COx claystone is a very low-permeability rock. Its mineral composition varies as a function of depth mainly due to geological sedimentary cycles (Lefranc et al. 2008) and the clay mineral content is roughly anti-correlated with the carbonate content. It corresponds to (Mohajerani 2011; Montes et al. 2004; Robinet et al. 2012, 2015; Sammartino et al. 2003): 20–60% of phyllosilicates (illite, interstratified illite/smectite, kaolinite, mica, chlorite), 10–40% of tectosilicates (quartz, feldspars), 15–80% of carbonates (calcite, dolomite), 0–3% of pyrite, iron oxides with less than one percent organic matter. The three main phases are clay minerals, quartz, and calcite. It is worth emphasizing that this argillite contains a high content of swelling clay minerals (smectites).

Table 1 Composition of ANDRA's synthetic water

Chemical element	Content (g/l)
NaCl	1.950
$NaHCO_3$	0.130
KCl	0.035
$CaSO_4,2H_2O$	0.630
$MgSO_4,7H_2O$	1.020
$CaCl_2,2H_2O$	0.080
Na_2SO_4	0.700

From the base to the top of the layer, the COx formation was divided into four lithostratigraphic units (C2a to C2d) and several petrophysical units (UA1, RIO, UA2, UA3, UT, USC1, RSO, and USC2) defined for the ANDRA project (Pellenard et al. 2014). The COx claystone consists mainly of three different layers to be more precise (Giot et al. 2019). There is the silto-carbonated unit (USC) which is on the top of the COx layer and is the most carbonated one. Its mineralogical composition is contrasted and variable; its porosity is about 15%. Then, there is the transition unit (UT), which is more homogeneous and with a clay content between 30 and 40%. The carbonate content increases from the bottom (20%) to the top (30%). Finally, there is the clay unit (UA), which is the most clayey unit, with clays, carbonate and quartz contents of about 45–50%, 27% and 24%, respectively.

The work of ANDRA (ANDRA 2005) showed that the pore space of the COx claystone represents about 18%. This porosity is made up of approximately 10% macropores (> 1 µm), 86% (0.1 µm to 1 µm) mesopores and 4% (< 1 µm) micropores according to the three classes listed in the work of Coll (2005). Initial stresses within the claystone are about 12 MPa at the level of the radioactive waste storage which corresponds to the lithostatic pressure at a depth of 500 m (Gratier et al. 2004). Water permeability tests (ANDRA 2005; Escoffier 2002) give values between 5.10^{-20} and 5.10^{-21} m^2.

The synthetic water of ANDRA, whose chemical composition is close to in situ porewater at the ANDRA URL, was used in our experiments. Its mineralogical composition is presented in the Table 1.

2.2 Experimental Device and Protocol

2.2.1 Samples Preparation

Cylindrical samples of 20 mm diameter and 40 mm height were used for the self-sealing tests. They were cored from ANDRA's boreholes. Each core sample was preserved in a bell jar (with water at the bottom) to keep its water saturation level above 90%. Before each test, the samples were artificially fractured. In the first step, they were sawn in two along a plane containing the axis of the cylinder, and in the second step, one of the faces was machined to obtain a crack on a one-third of the diameter whose opening was controlled as precisely as possible. The opening of the artificial crack was carried out by milling with a high-precision tool. This regular milling method allows the creation of an artificial space without generating significant damage. In fact, a small number of particles are extracted from the matrix until the desired depth is reached. It is worth emphasizing that artificial crack realization induces a drying of the crack tips, which is probably moderate given that this process is relatively fast (about half an hour). In addition, the crack is rapidly resaturated during the first stage of the self-sealing test.

For our tests, two orientations of the sample axis were considered, namely parallel and perpendicular to the bedding plane, to take into account the effect of the clay anisotropy. According to previous works (Auvray et al. 2015; Giot et al. 2019) and ANDRA's recommendations, we chose an aperture of 400 µm for the initial crack. We also tested a wider aperture (800 µm) to verify if self-sealing is also an efficient process for wide cracks. Figure 1 presents the geometry of the artificially cracked samples for both parallel and perpendicular orientations. Therefore, the initial crack has a theoretical initial volume equal to 106.5 mm^3 and 213 mm^3 for an aperture of 0.4 mm and 0.8 mm, respectively.

2.2.2 Experimental Device

We developed an innovative mini-triaxial cell with a height of 250 mm and a diameter of 100 mm in which cylindrical samples of a diameter of 20 mm and height of 40 mm can be tested. The particularity of this cell is that its body is made of PEEK CF30 (PolyEtherEtherKetone, 30% carbon fibers) and thus is transparent to X-rays, which made it possible to follow the evolution of the crack volume in the sample at different times under a high-resolution X-ray computed tomography (CT) scanner (Fig. 2). A confining pressure up to 12 MPa can be applied on the samples. At both end caps (outlets) of the cell, drainage holes allow to inject fluids (water or gas) at different pressures in the sample.

The fluids are injected with pressure generators (syringe pumps) into these outlets using flexible connections and injection circuit connectors in PEEK material, which allows a 360° rotation of the sample in the X-ray tomography, and then 3D scans of the sample before, during and after the self-sealing test. During self-sealing tests, upstream and downstream fluids pressures and exchanged fluid volumes are continuously recorded with our high-precision syringe pumps, thus allowing the continuous measurement of fluid flow rate and then crack permeability.

Table 2 References of the different samples with corresponding characteristics and experimental conditions

Samples	%$CaCO_3$	Solid grain density (g/cm^3)	Fracture opening (µm)	Orientation	Injected fluid	Temperature (°C)
EST60766-3	21	2.67	400	//	Water	20
EST62690-2	20.6	2.67	800	//	Water	20
EST63744-7	32	2.69	400	//	Water	20
EST63744-11	32	2.69	400	⊥	Water	20
EST66418-10	25.4	2.69	400	//	Water	80
EST66418-5	25.4	2.69	400	//	Water + gas	20
EST60007-71	52.8	2.71	400	⊥	Water	20
EST60018-71	5.3	2.61	400	⊥	Water	20
EST59996-71	68.1	2.71	400	⊥	Water	20

2.2.3 Experimental Protocols

The artificially fractured samples (isolated from the confining oil by a waterproof Viton© membrane) is put in the triaxial cell and then the hydrostatic stress (i.e., confining pressure) is then increased to 4 MPa, which corresponds to the pressure applied on the galleries wall by swelling clays (bentonite) of the plug. This confining pressure is kept constant during the whole test. Once the confining pressure is stabilized, an initial 3D X-ray scan is performed to record the initial shape of the crack. Just after, synthetic water is injected from the bottom (upstream) of the sample at a constant rate of 0.05 ml/min to saturate the fracture. As soon as the water comes out of the cell at the top (downstream), the injection is stopped and a 3D X-ray scan is performed to analyze the crack just after its saturation with water. Then, water circulation is imposed in the fractured sample with a water pressure gradient of 0.2 MPa (upstream/bottom pressure = 1 MPa; downstream/top pressure = 0.8 MPa), with a flow rate limit of 0.02 ml/min to avoid too fast water circulation and fracture damage. A scheme (with a cylindrical sample inside) and a photo of a triaxial compression cell made of PEEK are represented in Fig. 3. Once steady state flow is achieved with a stable gradient pressure of 0.2 MPa, water permeability can be measured. This is obviously impossible at the beginning of the self-sealing test because the crack permeability is infinite (the crack is totally open). So far, all these steps are performed at room temperature (~20 °C).

Concerning the self-sealing test under high temperature (80 °C in our case), the temperature is increased once the flow rate is stabilized. The temperature is controlled with a heating system around the triaxial cell (temperature-regulated bath). For this test, only one additional 3D X-ray scan is performed, at the end of the experiment once the temperature has cooled. Concerning the mixed self-sealing test with water and gas injection (at room temperature), the same procedure was followed, except that the gas is injected into the sample (from the bottom) at different times, with a bottom/upstream pressure of 0.2 MPa or 0.5 MPa (depending on the level of sealing), while the top/downstream is left at atmospheric pressure. During these gas injection stages, gas circulation removes first the water filling the crack and the tubing. Once the crack and the tubing are emptied, the gas can flow continuously through the sample. Then, once a steady state gas flow is achieved, gas permeability can be measured. The gas used for this experiment is nitrogen.

Nine samples were tested in total. The references of the different samples with corresponding characteristics and experimental conditions are given in Table 2. Each self-sealing test lasts at least one month.

2.2.4 3D X-Ray Tomography: Acquisition and Analysis of Voxel Data

The PEEK triaxial cell is placed in a GE Phoenix Nanotom S CT scanner (Fig. 1) and 3D scans with a relatively high voxel resolution of 24 µm are performed at different times during each self-sealing test. The resolution is limited by the size (diameter) of the peek triaxial cell which imposes a relatively large distance between the X-ray source and the detector. This scanner is equipped with a 180 kV micro-focus X-ray tube/generator and a CMOS 5 MPx detector. The scintillator type is: Hamamastu 2300 × 2300 CsI (iodure Cesium). The micro-focus and Flat CMOS systems enable high-definition X-ray images to be obtained at acquisition frequencies of 500 ms to several tens of minutes. The Phoenix CT scanner has an auto-protected chamber to enable safe access to the hydraulic circuits that generate the confining and water/gas injection pressures in the triaxial cell. The acquisition parameters are: 1500 projections, 3 images per projection, image every 1000 ms, exposure time 1000 ms, which allows us to have at the end of the scan 1500 projections, voltage of 120 kV and intensity of 200 µA of the rays.

After 3D reconstruction of the sample volume, images were analyzed with the VGStudio MAX Software (Volume Graphics GmbH). It allows to isolate and visualize

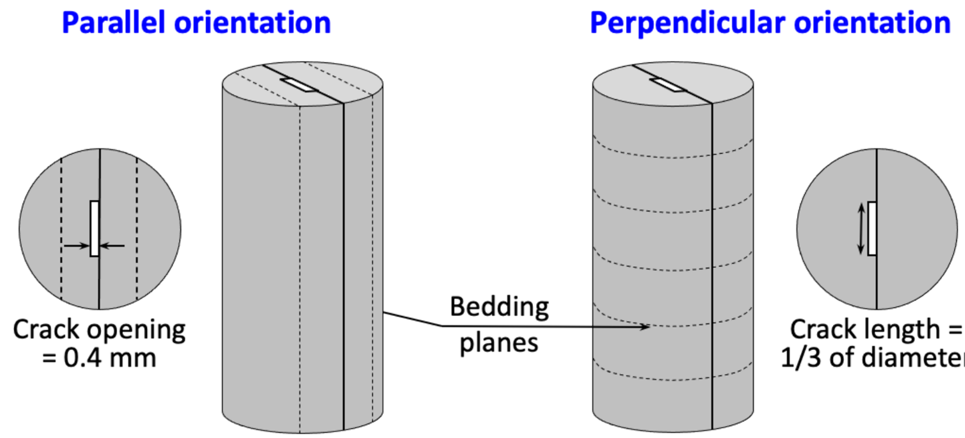

Fig. 1 Geometry of the artificially fractured cylindrical samples ($\varnothing = 20$ mm; $h = 40$ mm) for self-sealing tests

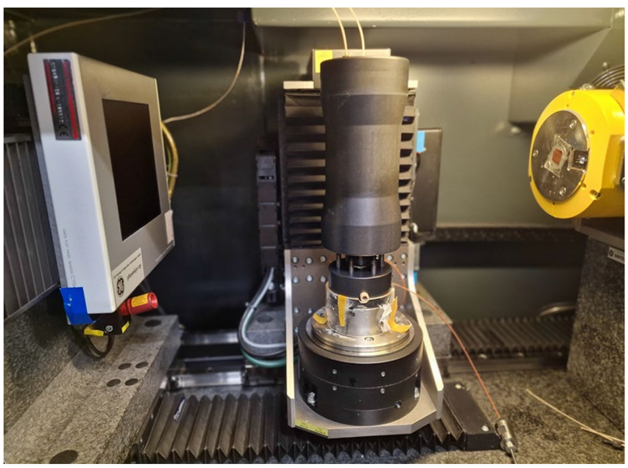

Fig. 2 PEEK triaxial compression cell for self-sealing tests in an X-ray nano-tomograph

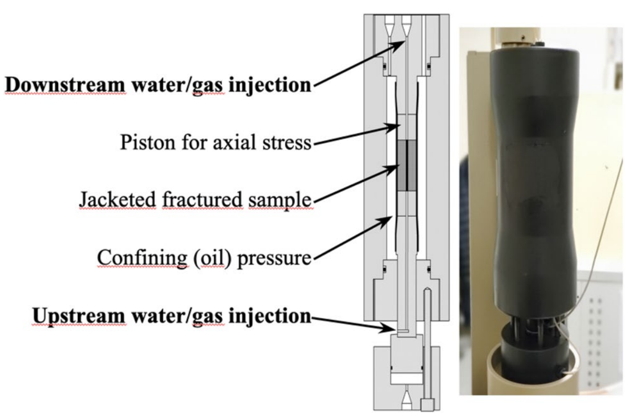

Fig. 3 Triaxial compression cell made of PEEK: scheme (with the cylindrical sample inside) and photo

the evolution of the fracture and to quantify the variations of its volume during the self-sealing test. The volume was estimated from the count of the voxels number assigned to the crack from the reconstructed sample. Here, the main issue was to discriminate the void from the rest of the sample after reconstruction (the void is filled with water). The method was based on porosity/inclusion analysis of VGSTUDIO MAX 3.5 working with the threshold only. Basically, it consists in:

- Overlay perfectly all the 3D scans of a sample using the tools of VGSTUDIO MAX 3.5: all the points are merged and put at the same scale. The only difference is at the crack surface.
- Determine the zone where the fracture is situated on the first 3D scan and extract this zone from all other scans.
- Once all the interest zones are extracted, determine the voids with the method based on porosity/inclusion analysis of VGSTUDIO MAX 3.5 with the threshold-only option on pore mode.

It is worth emphasizing that the software VG Studio Max helps the user to determine the threshold value. First, the user chooses the pixels corresponding to the background (voids or cracks in our case) and the pixels corresponding to the material (claystone in our case). Then, the software approximates the threshold value that varies from one scan to another. After all these steps are performed, the software gives us a lot of usable data such as total pore volume, connected pore volume, pore surface, and average pore radius. These pores represent the void in the crack (filled by water) and therefore allow us to have the volume of the crack during the self-sealing tests.

2.2.5 Permeability Measurements

The water permeability of the cracked samples was calculated from the volumes measured with the syringe pumps at both upstream and downstream sides of the sample during the self-sealing test. It is based on a steady-flow approach taking into consideration Darcy's law, which describes the flow across a porous medium induced by a pressure gradient:

$$k = \frac{Q\mu L}{S(P_u - P_d)} \tag{1}$$

where k is the intrinsic permeability (m^2), Q the volumetric flow rate (m^3 s^{-1}) measured at both upstream and downstream sides of the sample, μ the liquid (water in our case) dynamic viscosity (Pa.s), S the injection surface (cross section) of the sample (m^2), L the length of the sample (m), and P_u and P_d the upstream and downstream fluid pressures (Pa).

Since we are measuring the flow rate in a cracked porous sample and since the Darcy law describes the flow across a porous medium, the permeability k corresponds here to an "apparent permeability" of a cracked sample. But actually, since the matrix permeability of this claystone is very low (less than 10^{-20} m^2), the measured permeability corresponds probably to the crack permeability.

The gas permeability k (m^2) measured in the laboratory is calculated at equilibrium according to Darcy's equation for compressible gas flow:

$$k_a = \frac{2\mu Q L P_u}{S(P_u^2 - P_d^2)} \tag{2}$$

where P_u and P_d are the upstream and downstream gas (pore) pressures (Pa) respectively, Q is the volumetric flow rate (m^3 s^{-1}), μ the gas (nitrogen in our case) dynamic viscosity (Pa.s), S is the injection surface of the sample (m^2) and L the length of the sample (m).

Actually, this measured gas permeability is the apparent gas permeability. However, considering that the gas flow occurs mainly in a large fracture, the Klinkenberg or slippage effect (Klinkenberg 1941) is probably negligible here. Therefore, we can consider that the measured permeability is the intrinsic permeability and it represents the permeability of the fracture (the gas flow occurs mainly in the crack).

3 Experimental Results

3.1 Influence of the Sample Orientation on the Self-Sealing Process

To observe the influence of the sample orientation on the self-sealing process, self-sealing tests were carried out (at room temperature) on samples with different orientations, i.e., parallel (EST63744-7) and perpendicular (EST63744-11) to the bedding plane, but with the same calcium carbonate (calcite) content (32%) and the same crack opening (400 µm). The evolution of the water permeability and the 3D scans of these two tests are presented in Figs. 4, 5 and 6.

First, it is worth noting that the hydrostatic loading at a confining pressure of 4 MPa induces a partial closure of the initial crack. This mechanical closure is much more efficient for the parallel sample, probably because of the clay mineral's orientation. The sample saturation induces also a partial closure of the initial crack. Contrary to what was supposed, the self-sealing process doesn't seem more efficient for the parallel sample, i.e., when the bedding plane (and clay minerals alignment) is parallel to the axis of the sample and to the artificial fracture surface. This point will be discussed thereafter in the discussion section.

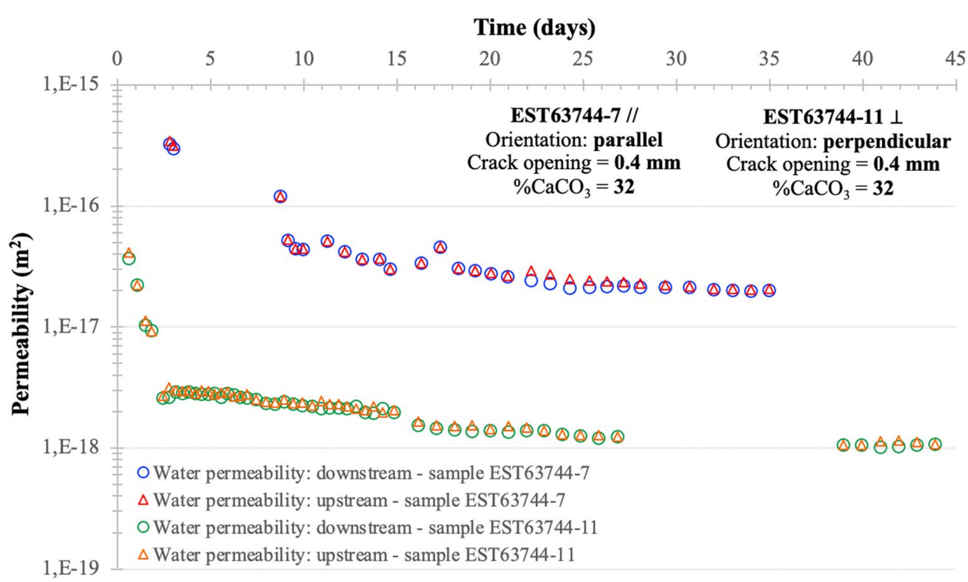

Fig. 4 Evolution of water permeability of parallel sample EST63744-7 and perpendicular sample EST63744-11 during a self-sealing test at 20 °C

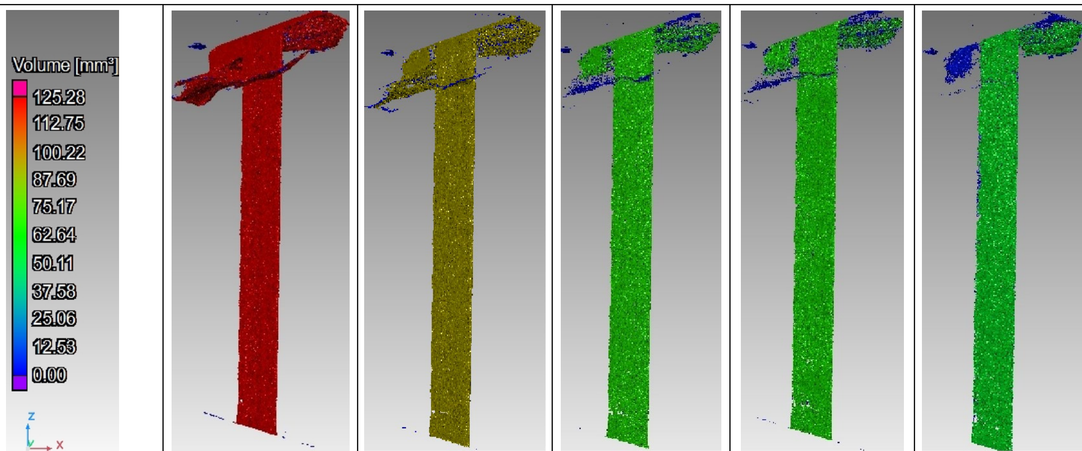

	Day 0-	Day 0+	Day 1	Day 2	Day 44
Volume (mm³)	126.2	96.0	70.7	69.4	60.8
%CaCO$_3$	32				

Fig. 5 X-ray 3D tomography images of perpendicular sample EST63744-11 showing the evolution of the crack volume with time (initial crack opening = 0.4 mm) during a self-sealing test at 20 °C (Day 0−: after hydrostatic loading; Day 0 +: after crack saturation)

	Day 0-	Day 0+	Day 1	Day 2	Day 3	Day 10	Day 21	Day 35
Volume (mm³)	67.7	64.9	62.1	60.2	55.8	38.5	34.2	33.5
%CaCO$_3$	32							

Fig. 6 X-ray 3D tomography images of parallel sample EST63744-7 showing the evolution of the crack volume with time (initial crack opening = 0.4 mm) during a self-sealing test at 20 °C (Day 0−: after hydrostatic loading; Day 0 +: after crack saturation)

3.2 Influence of the Calcite Content on the Self-Sealing Process

To observe the influence of the mineralogical composition (calcite content) of the COx on the self-sealing process, several tests were performed on core samples with an artificial crack aperture of 400 µm, parallel orientation, but with different carbonate contents. The self-sealing test performed on the specimen EST59996-71 with perpendicular orientation and a very high calcium carbonate content of 68.1%

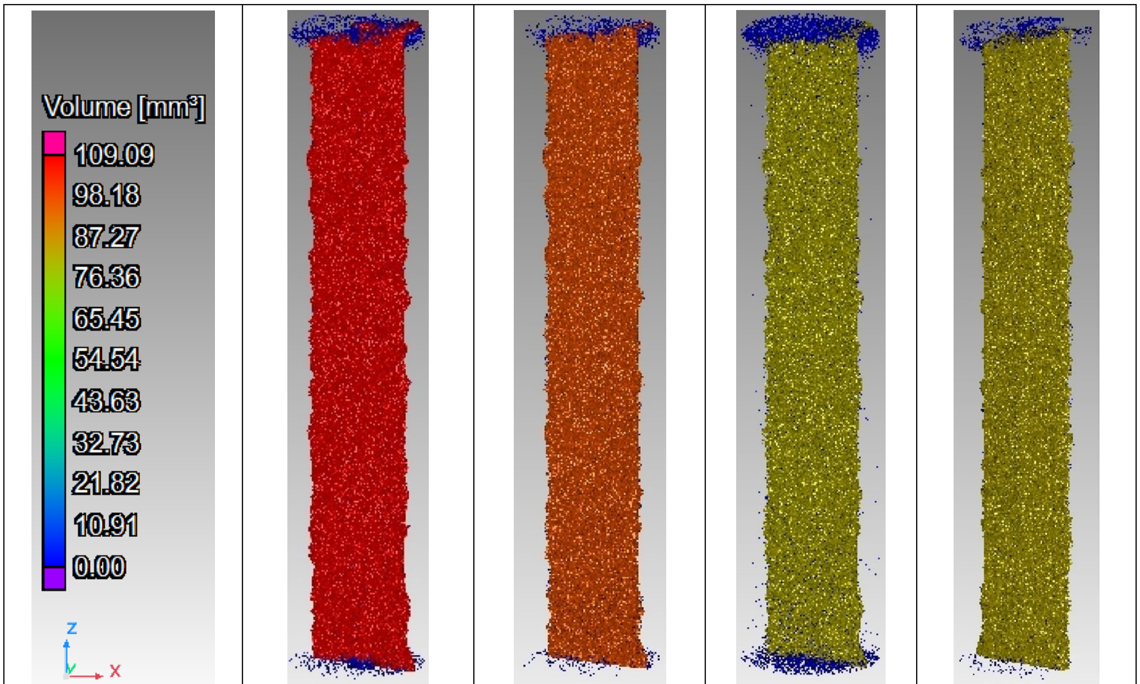

	Day 0-	Day 0+	Day 14	Day 42
Volume (mm^3)	110.8	98.5	86.8	84
%$CaCO_3$	68.1			

Fig. 7 X-ray 3D tomography images of perpendicular sample EST59996-71 showing the evolution of the crack volume with time (initial crack opening = 0.4 mm) during a self-sealing test at 20 °C (Day 0−: after hydrostatic loading; Day 0 +: after crack saturation)

(crack opening = 400 µm) lasted 42 days. Figure 7 shows the evolution of the fracture geometry obtained from the analysis of 3D X-ray tomography images. Before water saturation (just after hydrostatic loading), the fracture volume was equal to 111 mm^3. Just after crack saturation, it decreased to 98 mm^3. After 14 days of the self-sealing experiment, the volume decreased a little (87 mm^3). After 42 days, the volume was equal to 84 mm^3. Thus, self-sealing was very moderate and the fracture remained globally open. Therefore, no water permeability measurements of the fracture could be performed since the flow rate was too fast.

The self-sealing test performed on specimen EST60007-71 with perpendicular orientation and a high calcium carbonate content of 52.8% (crack opening = 400 µm) lasted 25 days. Figure 8 shows the evolution of the fracture geometry obtained from the analysis of 3D X-ray tomography images. The self-sealing test was also very moderate for this perpendicularly oriented sample and the fracture remained globally open, as for the very carbonated sample EST59996-71. Therefore, no water permeability measurements of the fracture could be performed for this carbonated sample.

The self-sealing test performed on specimen EST60018-71 with perpendicular orientation and a very low calcium carbonate content of 5.3% (crack opening = 400 µm) lasted 21.4 days. The very rapid sealing induced the plugging of the inlet capillary, making further water injection and permeability measurement impossible, and stopped the self-sealing process. Figure 9 shows the evolution of the fracture geometry obtained from the analysis of 3D X-ray tomography images. Before water saturation (just after hydrostatic loading), the fracture volume was equal to 60 mm^3. Immediately after water saturation, the fracture volume reduced to 40 mm^3 and it did not change until the end of the test, probably due to the plugged capillary as a result of the collapse in the crack due to the rapid swelling of clay minerals.

From these results, it seems obvious that the calcite content has a strong impact on the self-sealing process in argillite.

3.3 Influence of the Crack Aperture on the Self-Sealing Process

The influence of the crack opening was studied by performing self-sealing tests on clayey samples with the same low carbonate content (~ 20%), parallel orientation, but with different crack widths. The first one EST60766-3 has an artificial crack opening of 400 µm and a carbonate content of 21%. The second sample EST62690-2 has a crack opening of 800 µm and a carbonate content of 20.6%. The evolution

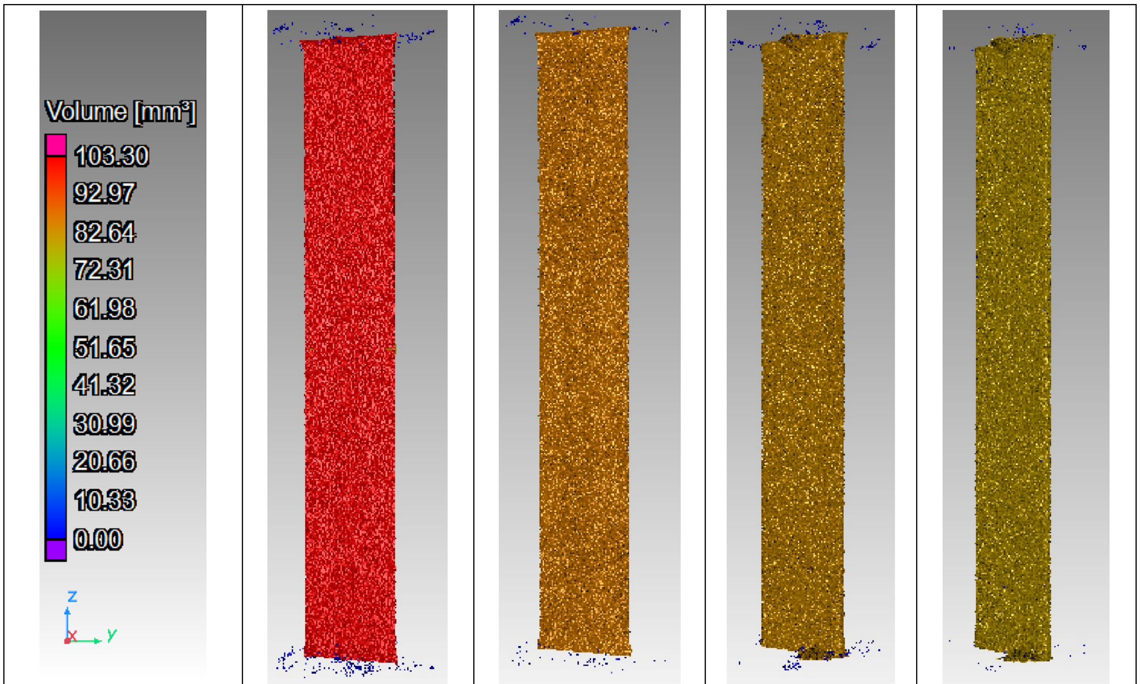

	Day 0	Day 4	Day 12	Day 25
Volume (mm^3)	103.6	86.2	83.7	81.0
%$CaCO_3$	52.8			

Fig. 8 X-ray 3D tomography images of perpendicular sample EST60007-71 showing the evolution of the crack volume with time (initial crack opening = 0.4 mm) during a self-sealing test at 20 °C (Day 0: after hydrostatic loading)

of the water permeability and the crack volumes of these two samples are represented in Figs. 10, 11 and 12.

It is noticed that the smaller the initial crack opening is, the faster the water permeability decreases. Indeed, the permeability of sample EST60766-3 with an initial crack opening of 0.4 mm decreased from 10^{-17} to 10^{-18} m^2 in 20 days, while the permeability of sample EST62690-2 with an initial crack opening of 0.8 mm decreased from 10^{-15} to less than 10^{-18} m^2 in 41 days. Concerning sample EST62690-2, the permeability data are missing from day 26 to day 40 because of a technical problem. A last permeability measurement was performed on day 41 and the test was stopped. At the end of this experiment, the permeability is even smaller than the permeability of sample EST60766-3. X-ray tomography images show that the smaller the initial crack opening is, the faster the crack closes. Also, at the end of the experiment, the crack is more closed in sample EST60766-3 with an initial crack opening of 0.4 mm than in sample EST62690-2 with an initial crack opening of 0.8 mm. These results seem obvious because it takes longer to fill a larger volume. However, it is worth emphasizing that the self-sealing mechanism is still efficient even for a wide fracture (although it takes a little longer), especially for these two samples that have a low carbonate content (~ 20%).

Generally, the water permeability decreases rapidly during the first hours of injection followed by a slower decrease. However, the initial permeability of the healthy (i.e., initial) claystone is never recovered. The final water permeability is around 10^{-18}–10^{-19} m^2 and it is higher by almost 2 orders of magnitude compared to the value of the intrinsic permeability of the healthy COx claystone which is estimated between 10^{-21} and 10^{-20} m^2, depending on the orientation of the sample (ANDRA 2005; Escoffier 2002; Giot et al. 2011, 2012, 2014; Homand et al. 2004). Concerning the crack volume, the self-sealing process induces a significant reduction but the crack is never completely closed, at least for the duration of our tests.

3.4 Influence of the Temperature on the Self-Sealing Process

The influence of temperature on the self-sealing process has been studied by performing a self-sealing test at 80 °C following the protocol described previously. This test was performed on a parallel sample (EST66418-10) with an artificial fracture of 400 µm and a carbonate content of 25.4%. The evolution of the water permeability during this test is presented in Fig. 13. Only the upstream curve was represented (the downstream curve is almost the

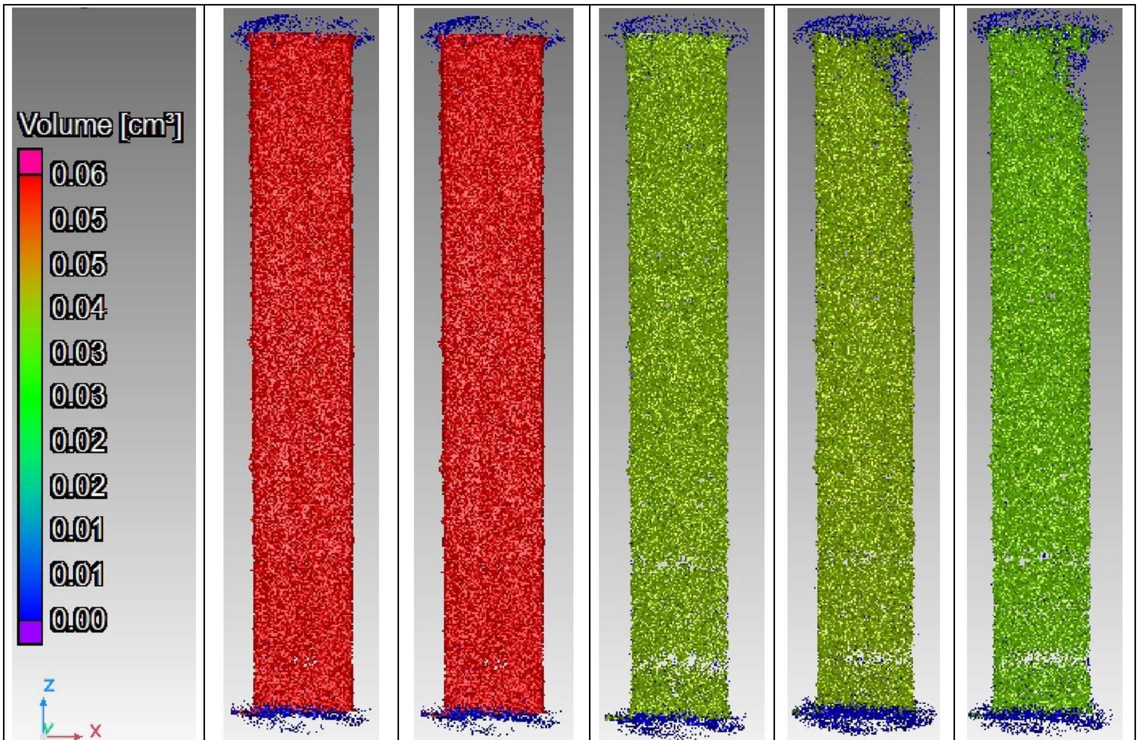

	Day 0-	Day 0+	Day 1	Day 3	Day 6
Volume (mm^3)	60	40	40	40	40
%$CaCO_3$	5.3				

Fig. 9 X-ray 3D tomography images of perpendicular sample EST60018-71 showing the evolution of the crack volume with time (initial crack opening = 0.4 mm) during a self-sealing test at 20 °C (Day 0−: after hydrostatic loading; Day 0 +: after crack saturation)

Fig. 10 Evolution of water permeability of parallel sample EST60766-3 and parallel sample EST62690-2 during a self-sealing test at 20 °C

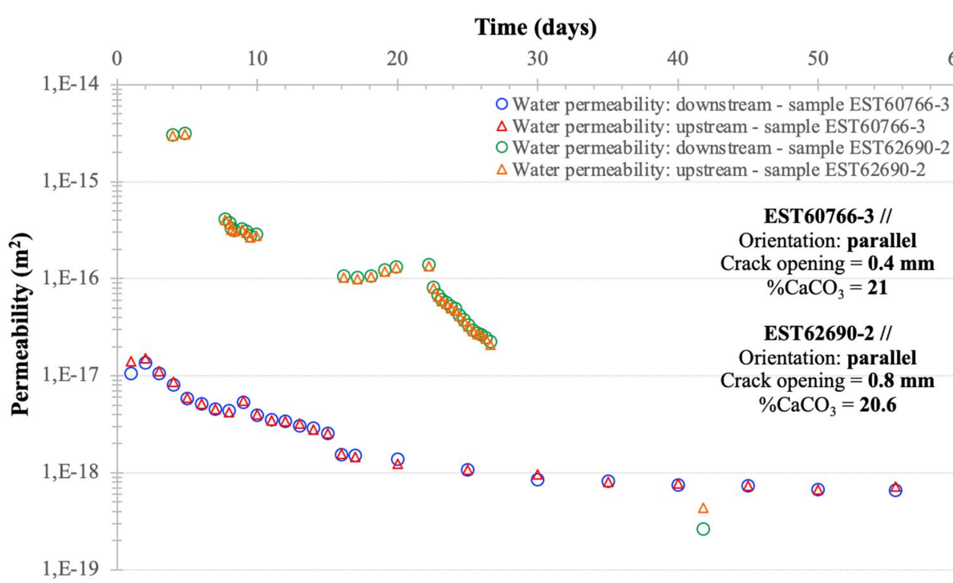

same) and it was compared with the upstream curve of the sample EST60766-3 (represented in Fig. 10), which is a similar sample but without a temperature increase. An increase of the water permeability just after the heating is observed, followed by a fast and then moderate decrease of the water permeability. Just after this rapid

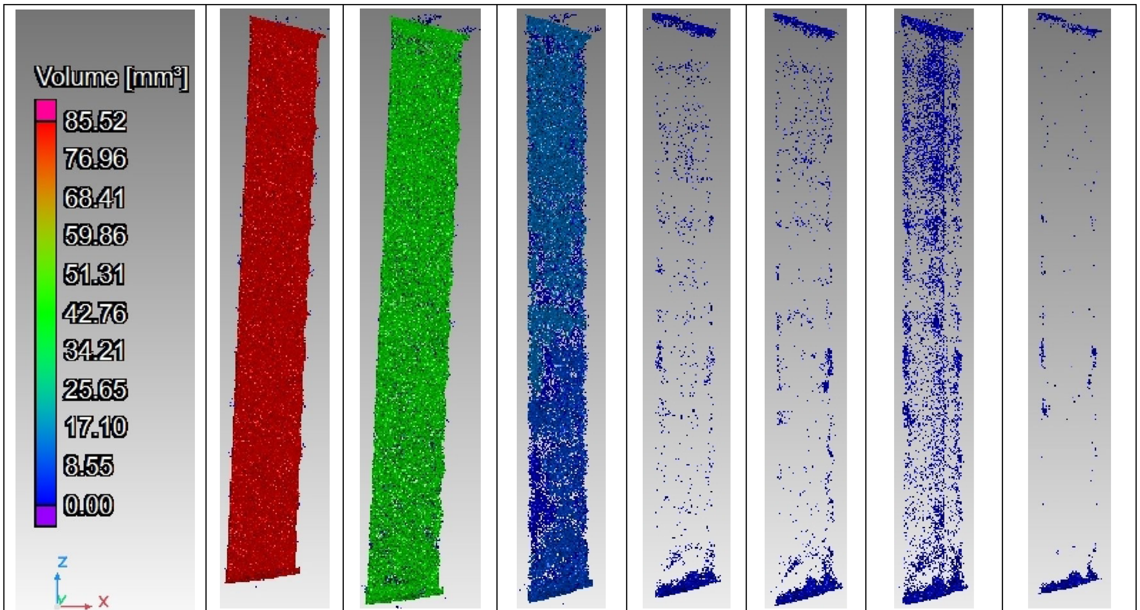

	Day 0-	Day 0+	Day 1	Day 2	Day 3	Day 8	Day 93
Volume (mm³)	85.6	44.2	26.4	2.3	2.2	5.4	1.0
%$CaCO_3$	21						

Fig. 11 X-ray 3D tomography images of parallel sample EST60766-3 showing the evolution of the crack volume with time (initial crack opening = 0.4 mm) during a self-sealing test at 20 °C (Day 0−: after hydrostatic loading; Day 0+: after crack saturation)

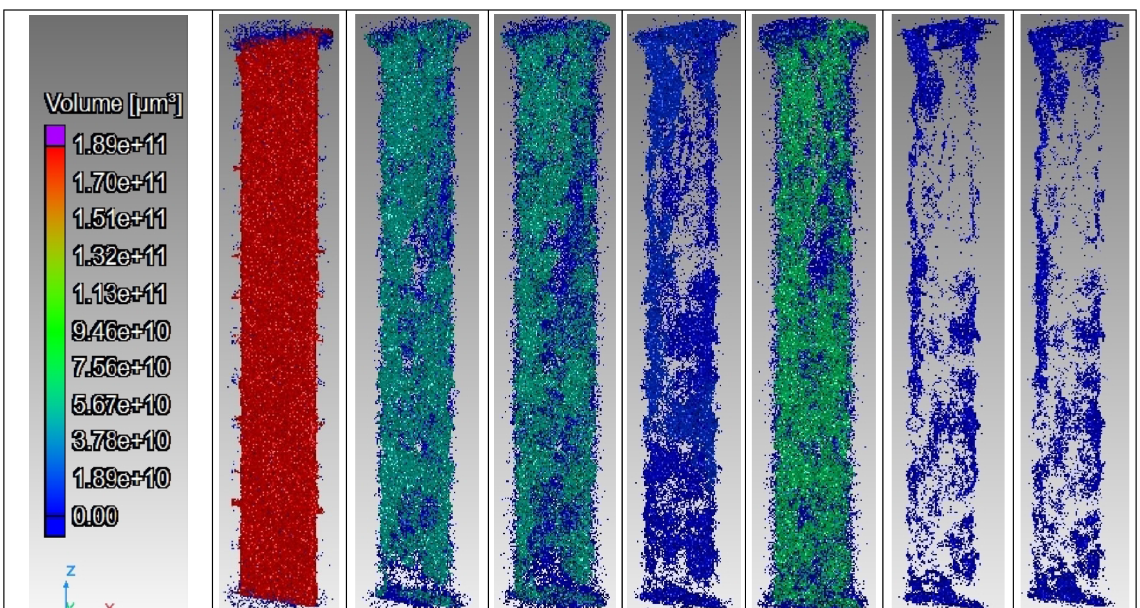

	Day 0	Day 2	Day 3	Day 10	Day 15	Day 20	Day 42
Volume (mm³)	191.0	58.3	64.2	26.9	78.2	9.5	10.6
%$CaCO_3$	20.6						

Fig. 12 X-ray 3D tomography images of parallel sample EST62690-2 showing the evolution of the crack volume with time (initial crack opening = 0.8 mm) during a self-sealing test at 20 °C (Day 0: after hydrostatic loading)

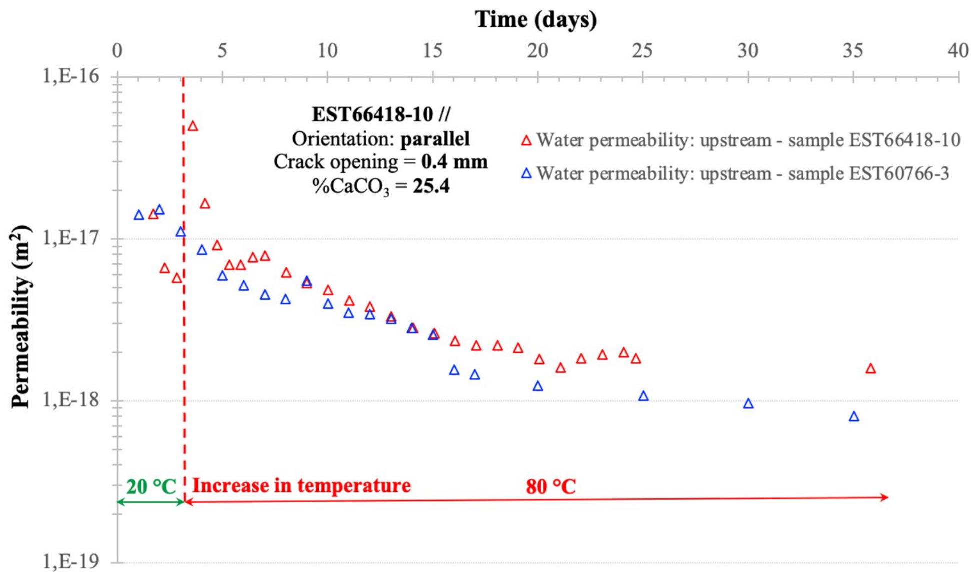

Fig. 13 Evolution of water permeability of parallel sample EST66418-10 during the self-sealing test at 80 °C compared to the permeability evolution of sample EST60766-3 (performed at 20 °C)

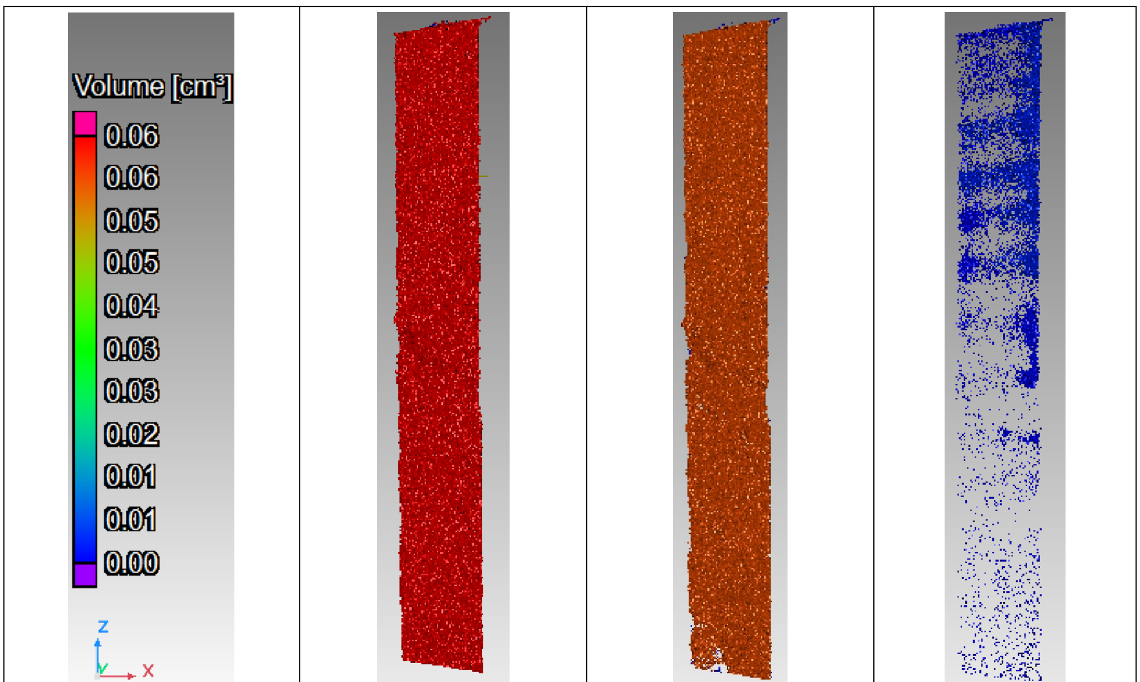

	Day 0-	Day 0+	Day 37
Volume (mm³)	60.0	60.0	10.0
%CaCO₃	25.4		

Fig. 14 X-ray 3D tomography images of parallel sample EST66418-10 showing the evolution of the crack volume with time (initial crack opening = 0.4 mm) during a self-sealing test at 80 °C (Day 0−: after hydrostatic loading; Day 0+: after crack saturation)

decrease, the water permeability drop follows the water permeability drop pattern observed in the other tests at room temperature (e.g., Fig. 10). Figure 14 shows the fracture geometry obtained from the 3D X-ray tomography data. Before water saturation (just after hydrostatic loading), the fracture volume was equal to 60 mm^3. After 37 days of self-sealing experiment, the volume decreased until 10 mm^3. It seems that temperature has a slight delay effect on the self-sealing process since the permeability

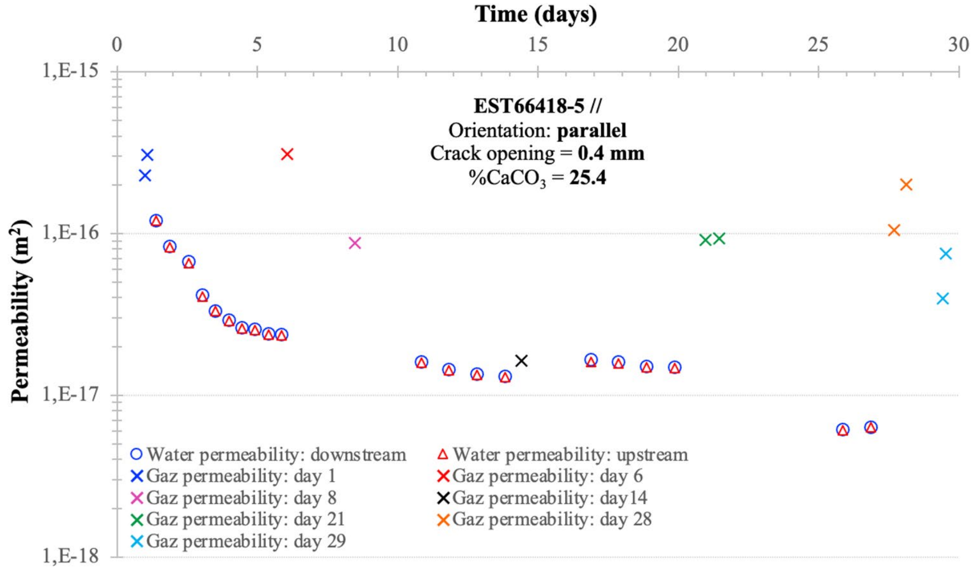

Fig. 15 Evolution of water and gas permeability of parallel sample EST66418-5 during the mixed self-sealing test with water and gas at 20 °C

and the volume of the crack decrease slower than for the similar test performed at 20 °C on the sample EST60766-3, as illustrated in Fig. 13 for the permeability.

3.5 Influence of Gas Injection on the Self-Sealing Process

A self-sealing test was performed with nitrogen injections to determine the influence of inert gas on the self-sealing process. The test was performed on a parallel sample (EST66418-5) with a 400 µm wide fracture and a carbonate content of 25.4%. The water and gas permeability of the specimen are presented in Fig. 15. It is worth emphasizing that there is a scattering of gas permeability measurements. There are many technical and physical reasons to explain this: the difficulty to obtain a measurable steady-state gas flow (the time interval is not the same for all gas permeability measurements), the difficulty to apply and measure precisely low gas pressures (0.2 MPa or 0.5 MPa) at the bottom/upstream of the triaxial cell, the residual water inside the crack that can disturb the gas flow. At the end of this self-sealing test, the water permeability is about 10^{-17} m^2, whereas the gas permeability is about 10^{-16} m^2. The difference is not that important.

It results that the water permeability decreases quite rapidly at the beginning like for the similar test EST60766-3 (e.g., Fig. 10) but the decrease is slower thereafter. In this case, also, the initial permeability of the healthy (i.e., initial) claystone is not recovered. It seems that the injection of the gas slows down the decrease of the water permeability even though the crack is almost closed at the end of the experiment after 29 days (Fig. 16).

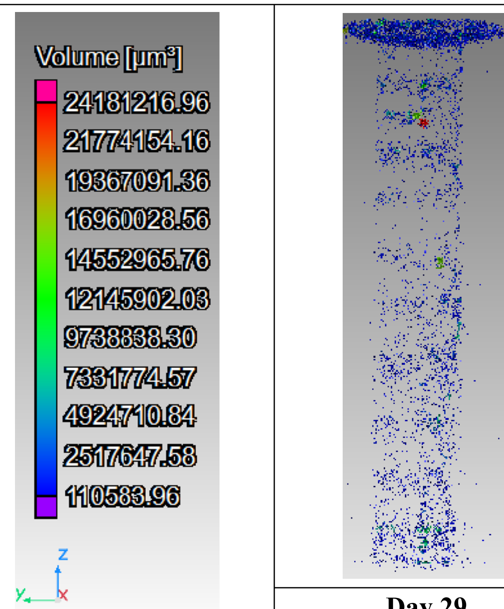

	Day 29
Volume (mm³)	3.3
%CaCO$_3$	25.4

Fig. 16 X-ray 3D tomography image of parallel sample EST66418-5) showing the crack volume at the end of a mixed self-sealing test with water and gas at 20 °C (initial crack opening = 0.4 mm)

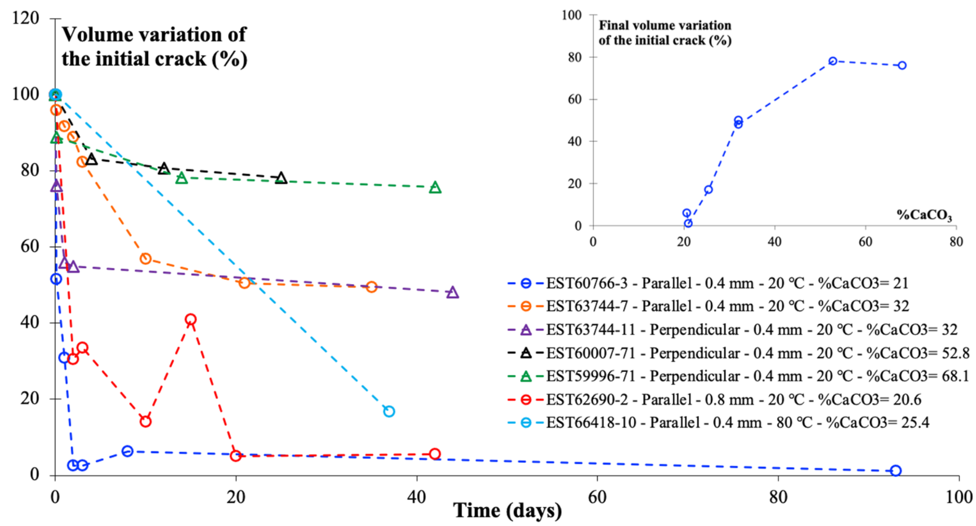

Fig. 17 Volume variation percentage of the initial crack (normalized with the volume after hydrostatic loading) obtained from X-ray tomography 3D images during all self-sealing tests with only water. Insert at the top right: volume variation percentage of the initial crack at the end of the test as a function of the calcite content

4 Discussion

4.1 Influence of the Calcite Content

The results of the different self-sealing tests that were carried out on the COx claystone seem to indicate that several parameters have an influence on the permeability reduction and closure of the initial artificial crack. The first parameter is the calcium carbonate (calcite) content. This parameter is roughly anti-correlated with the clay content. The results presented in Figs. 4 and 5 (EST63744-11, $\%CaCO_3 = 32$), 7 (EST59996-71, $\%CaCO_3 = 68.1$), 8 (EST60007-71, $\%CaCO_3 = 52.8$) and 9 (EST60018-71, $\%CaCO_3 = 5.3$) on perpendicular samples under 20 °C show that the carbonate content has a very significant influence on the physico-chemical sealing process. Indeed, the higher the carbonate content, the slower the self-sealing process. And for very high carbonate content, i.e., for very low clay content (sample EST59996-71, Fig. 7), there is almost no self-sealing. These processes are described in Auvray et al. (2015). This is very well illustrated in Fig. 17, which represents the volume variation percentage of the initial crack (normalized with the volume after hydrostatic loading) obtained from X-ray tomography 3D images during all self-sealing tests with only water. Only sample EST60018-71 wasn't represented in this Fig. 17 because the very rapid sealing induced the plugging of the inlet capillary and stopped the self-sealing process. Actually, whatever the sample orientation (parallel or perpendicular) this trend is verified. The insert in this Figure 17 represents the volume variation percentage of the initial crack at the end of the test (even though the test duration is not the same for all samples) as a function of the calcite content. It shows that the self-sealing capacity is strongly correlated to the calcite content. This result is very important because it highlights the importance of the mineralogy (i.e., clay and then carbonates content) of the clay host rock to allow a good sealing of fractures in the EDZ during the resaturation of the underground structures for radioactive waste storage in clayey rocks, which will guarantee the safety of the site.

Concerning the most carbonated samples EST59996-71 ($\%CaCO_3 = 68.1$) and EST60007-71 ($\%CaCO_3 = 52.8$), the crack volume barely changed during the self-sealing experiments (Figs. 7, 8 and 17) and it was not possible to measure the water permeability because the crack remained completely open, which prevented obtaining a stable pressure gradient. Contrarywise, concerning the most clayey sample 60,018–71 ($\%CaCO_3 = 5.3$), the sealing process was very rapid, almost instantaneous actually (Figs. 9 and 17), which induced the plugging of the inlet capillary and didn't allow permeability measurements. Concerning the samples with intermediate carbonate content, whatever the initial crack aperture, orientation and temperature, i.e., EST63744-11 ($\%CaCO_3 = 32$), EST63744-7 ($\%CaCO_3 = 32$), EST60766-3 ($\%CaCO_3 = 21$), EST62690-2 ($\%CaCO_3 = 20.6$) and EST66418-10 ($\%CaCO_3 = 25.4$), it was possible to measure the water permeability (Figs. 4, 10 and 13) during the self-sealing experiments. These permeability measurements, as well as the analysis of the evolution of cracks volume (Figs. 5, 6, 7, 8, 11, 12, 14 and 17), support the work of Giot et al. (2019) where it is indicated that the threshold regarding the carbonate content to observe self-sealing would be around 40%. Below this threshold, self-sealing process is effective, but almost non-existent when the carbonate content is above. The value of this threshold is consistent with the evolution of the volume variation percentage of the initial crack at the end of the test as a function of the calcite content, which is represented in the insert of Fig. 17.

4.2 Influence of Sample Orientation and Crack Aperture

The X-ray tomography 3D images (Figs. 5 and 6) and permeability measurements (Fig. 4) obtained on samples EST63744-11 (perpendicular, $\%CaCO_3 = 32$) and EST63744-7 (parallel, $\%CaCO_3 = 32$) didn't provide evidence for the influence of anisotropy on the self-sealing process. These two core samples were taken from the same borehole EST63744 (same mineralogical and petrophysical parameters, therefore), have the same initial crack opening (400 µm) but are oriented differently, i.e., perpendicularly and in parallel to the bedding plane, respectively. First, the initial mechanical closure due to the initial hydrostatic loading with a confining pressure of 4 MPa induces the closure of the artificial crack, whose theoretical initial volume is equal to 106.5 mm^3. This mechanical closure is much more efficient for the parallel sample, probably because of the clay minerals orientation which is parallel to the crack surface (and to the cylindrical sample axis).

Second, concerning the self-sealing process, Auvray et al. (2015) suggested that it is more efficient for parallel orientation than for perpendicular orientation, even though their statement is not obvious considering the experimental curves presented in their paper. Giot et al. (2019) proposed that the first phase of the self-sealing process is due to the crystalline swelling of smectite clay minerals, by adsorption of water in the clay sheets since the samples are partially saturated (actually a little desaturated in our case), before the self-sealing experiment starts (i.e., during the initial crack saturation stage). Then, during the self-sealing experiment, follows an osmotic swelling of the clay minerals, by absorption of water between clay particles at higher water saturation. The third and final phase is the formation of the first clay plugs. Samples oriented in parallel to the bedding plane have water infiltrating more easily between the sheets, and this initiate the self-sealing process more quickly. During these quick phases, there is a rapid decrease in the water permeability and the crack volume. Then, there is a moderate and progressive decrease in water permeability and crack opening due to the progressive swelling of smectite clay minerals in the whole sample from the artificial central crack to the sample borders, and the expansion and densification of clay plugs.

From that, one can suppose for the parallel samples, that clay minerals can swell freely laterally towards the inside of the fracture without any constraint. Contrariwise, when the sample axis is perpendicular to the bedding plane, one can suppose that the axial contraction (due to the 4 MPa confining pressure in our case) prevents a free swelling of the clay minerals surfaces in the axial direction and the swelling in the lateral direction (i.e., perpendicular to the crack surfaces) is probably not that significant. For all self-sealing tests performed with only water injection at room temperature (20 °C), the same evolution of the water permeability and the crack volume was globally observed and the physical mechanisms describes above could explain this evolution. However, the influence of sample orientation is not obvious in our experimental results and it seems that the self-sealing process is equally efficient for both parallel and perpendicular orientations. The (crystalline and osmotic) swelling mechanisms are certainly more efficient in the parallel samples than in the perpendicular samples, but the final phases of plugs formation, expansion and densification, which are maybe less dependent on the sample orientation, are possibly much more efficient to seal cracks. This could explain why, finally, there is no significant influence of the sample orientation in our self-sealing experiments. Obviously, this conclusion has to be verified with additional self-sealing tests.

The X-ray tomography 3D images (Figs. 11 and 12) and the permeability measurements (Fig. 10) obtained on samples EST60766-3 (parallel, $\%CaCO_3 = 21$, initial crack opening = 0.4 mm) and EST62690-2 (parallel, $\%CaCO_3 = 20.6$, initial crack opening = 0.8 mm) provide evidence for the influence of initial crack opening on the self-sealing process. These experiments showed that the sample with a crack opening of 400 µm self-seals faster than the sample with a larger crack opening (800 µm), which is also illustrated in Fig. 17. But at the end of both experiments, the permeability is almost the same (~ 10^{-18} m^2). Even though this result has to be verified with additional similar experiments, it is obvious because it takes longer to fill larger volume, while the swelling speed of the swelling clay minerals is probably the same in both cases. As explained by Giot et al. (2019), water must infiltrate the sheets to make them swell. So, when the two crack lips are closer, the crack closes faster and therefore the value of the water permeability and the opening of the crack reduce faster. Moreover, the permeability evolution of sample EST62690-2 with an initial crack opening of 0.8 mm (Fig. 10) has a non-monotonic trend. This means that fracture self-sealing is not a continuous and linear mechanism if the crack opening is wide. Indeed, in that case (wide aperture), some sealing material can be torn off due to the water flow, which can occasionally increase the permeability.

4.3 Influence of Temperature and Gas

The self-sealing test performed with water injection at a high temperature (80 °C) on the sample EST66418-10 (parallel, $\%CaCO_3 = 25.4$, initial crack opening = 0.4 mm) showed that just after the temperature rise, a rapid increase of the water permeability (Fig. 13). It is worth emphasizing that the water viscosity has been updated to take into account this temperature change (Eq. 1). This rapid increase can be explained by the water overpressure inside the fracture, which spreads the fracture lips and thus increases the water permeability of the fracture. Indeed, the coefficient of thermal expansion of water (2.6×10^{-4} (°C)$^{-1}$ at 25 °C and 5.8×10^{-4} (°C)$^{-1}$ at 80 °C) is an order of magnitude greater than that of solid grains in the COx claystone (2.6×10^{-5} (°C)$^{-1}$ at 25 °C and 11×10^{-5} (°C)$^{-1}$ at 80 °C) (Mohajerani 2011). This pore water overpressure inside the fracture (induced by this differential thermal expansion) dissipates thereafter as soon as drained conditions are restored. Therefore, the rapid increase in fracture permeability is transient. Thereafter, the permeability (Fig. 13) and the crack volume (Figs. 14 and 17) behave like for the other tests, i.e., decrease first rapidly, then slowly and progressively. It seems that temperature has a delay effect on the self-sealing process, when compared with the results of sample EST60766-3 (parallel, $\%CaCO_3 = 21$, initial crack opening = 0.4 mm) presented in Figs. 10 and 11, which is a similar sample but without temperature increase. This is well illustrated in Figs. 13 and 17 which show that the permeability and the crack volume decrease slower for the sample EST66418-10 than for the sample EST60766-3. However, this result has to be confirmed by additional similar experiments at high temperatures.

The mixed self-sealing test carried out with water and gas (nitrogen) on the sample EST66418-5 (parallel, $\%CaCO_3 = 25.4$, initial crack opening = 0.4 mm) showed the influence of the injection of an inert gas on the self-sealing process. The gas injection slows down the decrease of the water permeability (Fig. 15) even though the crack is almost closed at the end of the experiment after 29 days (Fig. 16). This could be explained by the desaturation of the crack induced by the gas injection, which thus reduces the self-sealing process. The injection of an inert gas has therefore a retarding effect on the self-sealing process. This result has also to be confirmed by additional similar experiments.

5 Conclusions and Perspectives

In this paper, the influence of different parameters on the self-sealing process in the Callovo-Oxfordian claystone was shown. With our X-ray transparent triaxial cell, and our experimental setup, it was possible to follow the evolution of the volume (with X-ray tomography 3D images) and the water permeability of cylindrical core samples of the COx claystone that were initially fractured artificially. Two kinds of self-sealing tests were performed. First, self-sealing tests with water injection under different temperatures, sample orientations, calcite contents and initial crack openings. Second, a mixed self-sealing test with an injection of both water and gas. 3D X-ray scans have been performed on all tested samples before, during and after the experiment and the voxel data were analyzed with high-end software for the visualization and analysis of computed tomography (CT) data to estimate the evolution of the crack volume. Also, water and gas permeability has been measured continuously during all tests.

It resulted first from our study that the mineralogical composition of the COx claystone influences the self-sealing process. The higher the calcium carbonate content (and therefore the lower the clay content), the less effective the self-sealing process, whatever the sample orientation (parallel or perpendicular). To have an effective sealing, it is necessary to have a carbonate content lower than 40%. Second, the mechanical closure is much more efficient for the parallel sample because of the clay minerals orientation (bedding plane) which is parallel to the crack surface. The clay sheets oriented in parallel to the initial artificial crack surfaces (lips), and then parallel to the cylindrical core sample axis and water flow direction, favor probably a faster swelling of crack surfaces. However, the influence of sample orientation is not obvious in our experiments and it seems that the self-sealing process is equally efficient for both parallel and perpendicular orientations. Third, the opening of the initial artificial crack influences the kinetic of the self-sealing process. It is faster for an initial crack opening of 400 μm than 800 μm. Finally, temperature and gas injection have a delay effect (rather slight in the case of temperature) on the self-sealing process. In the latter case, this is due to the crack desaturation which slows down the self-sealing process. Generally speaking, the self-sealing process is fast at the beginning of the test and then stabilizes after one month. Thanks to the self-sealing process, the permeability of the COx claystone samples is partially restored (~ 10^{-18}–10^{-19} m^2) compared to the initial permeability of the healthy (i.e., without fracture) claystone (~ 10^{-20}–10^{-21} m^2). It is all the more promising that the duration of our experiments is much shorter than the in situ time scale.

In all our experiments, whatever the experimental conditions, self-sealing is always an efficient mechanism if the clay content is high enough. These first results are very promising and give confidence to the positive impact of the self-sealing process on the restoration of the initial mechanical and hydraulic (i.e., sealing) properties of the clay host rock. This physico-chemical mechanism will allow a good sealing of fractures in the EDZ during the resaturation of the underground structures for radioactive waste storage in clayey rocks, which will guarantee the safety of the site. However, our first results have to be confirmed with additional similar experiments to better analyze the impact of some parameters on the self-sealing process, in particular sample orientation, temperature and gas injection.

Acknowledgements This project has received funding from the European Union's Horizon 2020 research and innovation program under grant agreement No 847593. Part of this work was financially supported by ANDRA (French National Radioactive Waste Management Agency), whom we thank for their participation. The experiments presented in this study were carried out with the experimental devices available in the HGM experimental platform (Université de Lorraine-CNRS—http://georessources.univ-lorraine.fr/fr/content/hydrogeomecanique).

Data availability Data will be available on request.

Declarations

Conflict of Interest The authors have no conflicts of interest to declare that are relevant to the content of this article.

References

ANDRA, 2005. Evaluation of the feasibility of a geological repository in an argillaceous formation (Dossier 2005Argile). Report Series.

Auvray C, Grgic D, Morlot C, Fourreau E, Talandier J. (2015). X-Ray Tomography Applied to Self-Healing Experiments on Argillites. 13th ISRM International Congress of Rock Mechanics, Montréal, (Québec, Canada)

Bastiaens W, Bernier F, Li XL (2007) SELFRAC: experiments and conclusions on fracturing, self-healing and self-sealing processes in clays. Phys Chem Earth Parts a/b/c 32(8–14):600–615. https://doi.org/10.1016/j.pce.2006.04.026

Bock H, Dehandschutter B, Derek Martin C, Mazurek M, de Haller A, Skoczylas F, Davy C (2010) Selfsealingof fractures in argillaceous formations in the context of geological disposal of radioactive waste – Reviewand synthesis. OECD Publications, Paris. ISBN 978-92-64-99096-1.

Coll C. (2005). Endommagement des roches argileuses et perméabilité induite au voisinage d'ouvrages souterrains [PhD Thesis]. Université Joseph-Fourier - Grenoble I

De La Vaissière R, Armand G, Talandier J (2015) Gas and water flow in an excavation-induced fracture network around an underground drift: a case study for a radioactive waste repository in clay rock. J Hydrol 521:141–156. https://doi.org/10.1016/j.jhydrol.2014.11.067

Escoffier S. (2002). Caractérisation expérimentale du comportement hydromécanique des argilites de Meuse/Haute-Marne [PhD Thesis]. Institut National Polytechnique de Lorraine

Giot R, Giraud A, Auvray C, Homand F, Guillon T (2011) Fully coupled poromechanical back analysis of the pulse test by inverse method. Int J Numer Anal Meth Geomech 35(3):329–359. https://doi.org/10.1002/nag.897

Giot R, Giraud A, Guillon T, Auvray C (2012) Three-dimensional poromechanical back analysis of the pulse test accounting for transverse isotropy. Acta Geotech 7(3):151–165. https://doi.org/10.1007/s11440-012-0158-7

Giot R, Giraud A, Auvray C (2014) Assessing the Permeability in Anisotropic and Weakly Permeable Porous Rocks Using Radial Pulse Tests. Oil Gas Sci Technol Revue d'IFP Energies Nouvelles 69(7):1171–1189. https://doi.org/10.2516/ogst/2013146

Giot R, Auvray C, Talandier J (2019) Self-sealing of claystone under X-ray nanotomography. Geol Soc London Special Publ 482(1):213–223. https://doi.org/10.1144/SP482.4

Gratier JP, Jenatton L, Tisserand D, Guiguet R (2004) Indenter studies of the swelling, creep and pressure solution of Bure argillite. Appl Clay Sci 26(1):459–472. https://doi.org/10.1016/j.clay.2003.12.035

Homand F, Giraud A, Escoffier S, Koriche A, Hoxha D (2004) Permeability determination of a deep argillite in saturated and partially saturated conditions. Int J Heat Mass Transf 47(14):3517–3531. https://doi.org/10.1016/j.ijheatmasstransfer.2004.02.012

Klinkenberg, L. J. (1941). The permeability of porous media to liquids and gases. Drilling and Production Practice. 200–213

Lefranc M, Beaudoin B, Chilès JP, Guillemot D, Ravenne C, Trouiller A (2008) Geostatistical characterization of Callovo-Oxfordian clay variability from high-resolution log data. Phys Chem Earth Parts a/b/c 33:S2–S13. https://doi.org/10.1016/j.pce.2008.10.053

Mohajerani M. (2011). Etude expérimentale du comportement thermo-hydro-mécanique de l'argilite du Callovo-Oxfordien [PhD Thesis]. Université Paris-Est

Montes HG, Duplay J, Martinez L, Escoffier S, Rousset D (2004) Structural modifications of Callovo-Oxfordian argillite under hydration/dehydration conditions. Appl Clay Sci 25(3):187–194. https://doi.org/10.1016/j.clay.2003.10.004

Pellenard P, Tramoy R, Pucéat E, Huret E, Martinez M, Bruneau L, Thierry J (2014) Carbon cycle and sea-water palaeotemperature evolution at the middle-late Jurassic transition, eastern Paris Basin (France). Mar Pet Geol 53:30–43. https://doi.org/10.1016/j.marpetgeo.2013.07.002

Robinet J-C, Sardini P, Coelho D, Parneix J-C, Prêt D, Sammartino S, Boller E, Altmann S (2012) Effects of mineral distribution at mesoscopic scale on solute diffusion in a clay-rich rock: example of the Callovo-Oxfordian mudstone (Bure, France). Water Resour Res. https://doi.org/10.1029/2011WR011352

Robinet J-C, Sardini P, Siitari-Kauppi M, Prêt D, Yven B (2015) Upscaling the porosity of the Callovo-Oxfordian mudstone from the pore scale to the formation scale; insights from the 3H-PMMA autoradiography technique and SEM BSE imaging. Sed Geol 321:1–10. https://doi.org/10.1016/j.sedgeo.2015.02.007

Sammartino S, Bouchet A, Prêt D, Parneix J-C, Tevissen E (2003) Spatial distribution of porosity and minerals in clay rocks from the Callovo-Oxfordian formation (Meuse/Haute-Marne, Eastern France)—Implications on ionic species diffusion and rock sorption capability. Appl Clay Sci 23(1):157–166. https://doi.org/10.1016/S0169-1317(03)00098-X

Van Geet M, Bastiaens W, Ortiz L (2008) Self-sealing capacity of argillaceous rocks: Review of laboratory results obtained from the SELFRAC project. Phys Chem Earth Parts a/b/c 33:S396–S406. https://doi.org/10.1016/j.pce.2008.10.063